



To effectively drive the conversion of sulfur with electroactive niobium tungsten oxide microspheres for lithium–sulfur battery

Lu Wang, Zhen-Yu Wang, Jun-Feng Wu, Guo-Ran Li, Sheng Liu, Xue-Ping Gao*

Institute of New Energy Material Chemistry, School of Materials Science and Engineering, Renewable Energy Conversion and Storage Center, Nankai University, Tianjin, 300350, China

ARTICLE INFO

Keywords:

Lithium–sulfur battery
Cathode
Niobium tungsten oxides
Lithium storage materials
Sulfur conversion

ABSTRACT

Realizing high energy density is the desirable target of the research and development for lithium–sulfur battery. However, the demands of high sulfur content in composite, high sulfur loading in electrode, and low electrolyte usage are likely excessive for reaching both high gravimetric and volumetric capacities of sulfur cathode with conventional inactive hosts of sulfur. Herein, in order to effectively drive the conversion of sulfur, niobium tungsten oxide ($\text{Nb}_{18}\text{W}_{16}\text{O}_{93}$) microspheres are adopted as electroactive host in the similar electrochemical window to sulfur. As expected, $\text{Nb}_{18}\text{W}_{16}\text{O}_{93}$ shows good electrochemical activity for lithium storage, and strong adsorption toward polysulfides. In particular, the in-situ electrochemically lithiated oxide in the discharge process can serve as good electrocatalyst and lithium-transfer bridge, facilitating the conversion of both the solid sulfur and soluble polysulfides. Correspondingly, the new lithium-transfer mechanism on $\text{Nb}_{18}\text{W}_{16}\text{O}_{93}$ endows the sulfur cathode a high areal capacity ($19.19 \text{ mAh cm}^{-2}$) under both high sulfur loading (16.94 mg cm^{-2}) and low electrolyte/sulfur ratio ($4.5 \mu\text{L mg}^{-1}$). In addition, the sulfur-based composite with high tap density (1.56 g cm^{-3}) shows a desired volumetric capacity ($1605.3 \text{ mAh cm}^{-3}$ -composite), almost 1.9 times of that for the conventional S/carbon composite. This work provides a new perspective for understanding the electroactive hosts in lithium–sulfur battery.

1. Introduction

The ever-increasing demands of portable electronics and electric vehicles call eagerly for high-energy storage devices, and have set off an upsurge of research in novel secondary batteries [1–3]. Lithium–sulfur (Li–S) battery has become one of the primary focus, owing to its high theoretical energy density (2600 Wh kg^{-1}) [4–6]. However, two tricky problems need to be settled before truly realizing the high energy density at the cell level. One is the sluggish redox kinetics of the multi-step conversion of sulfur, which would cause large polarization and low utilization of active materials [7–10]. The other problem is unsatisfactory cycle performance caused by the severe “shuttle effect” of the soluble intermediate polysulfides (LiPS). These problems could be magnified dozens of times under high sulfur loading and low electrolyte usage, which are necessary to achieve high energy density of Li–S battery.

Aiming at these problems, great efforts have been made to motivate the development of Li–S battery. Usually, carbon-based nanomaterials are widely used as sulfur host to provide a good conductive network for

the conversion of the insulated sulfur, and confine soluble LiPS mainly by physical interactions [11–16]. However, the intrinsic low density and large porosity of those carbon nanomaterials are adverse to the volumetric capacity of the cathode, which require excessive electrolyte simultaneously to wet the interface of porous electrode.

Introducing the carbon-free polar hosts with catalytic activity could be a feasible way for constructing compact cathodes with the low electrolyte usage [17–21]. Various metal compounds, such as metal nitrides [22–25], metal sulfides [8,26–30], and metal oxides [20,21,31–33] are used to enhance the electrochemical performance by virtue of polar adsorption and catalytic conversion toward soluble LiPS. However, to truly realize both the high gravimetric and volumetric capacities, high sulfur content in composite, high sulfur loading in cathode, and low electrolyte usage are essential, which in turn will cause the slow mass/electron transport, sluggish redox kinetics, and unsatisfied electrochemical performance. Therefore, it would be preferable to accelerate the redox kinetics of the sulfur cathode, and enhance the mass/electron transport in porous electrode simultaneously by adopting desirable host. In most cases, the host materials reported previously are

* Corresponding author.

E-mail address: xpgao@nankai.edu.cn (X.-P. Gao).

<https://doi.org/10.1016/j.nanoen.2020.105173>

Received 3 June 2020; Received in revised form 1 July 2020; Accepted 3 July 2020

Available online 25 July 2020

2211-2855/© 2020 Elsevier Ltd. All rights reserved.

electrochemically inactive during the discharge/charge process of the sulfur cathode. If the electro-active materials are adopted as the sulfur host in the working potential window, it would not only help to increase the capacity of the sulfur cathode, but also manipulate the electrochemical conversion kinetics of the solid sulfur and soluble LiPS.

As demonstrated recently, some niobium tungsten oxides are good electrochemical lithium storage materials with certain reversible capacity and high-rate capability [34–37], due to the multiple redox couples (W^{6+}/W^{5+} and $Nb^{5+}/Nb^{4+}/Nb^{3+}$) and high diffusion coefficient of Li-ions ($10^{-13} \text{ m}^2 \text{ s}^{-1}$). In particular, the electrochemical window of niobium tungsten oxides for lithium storage is in the potential region of 1–3 V, coincidentally covering the conversion of sulfur in the potential region of 1.7–2.8 V. Herein, $Nb_{18}W_{16}O_{93}$ (NWO) with excellent rate performance and slightly lower lithiation potential than sulfur, is adopted as the electroactive sulfur host. It is expected that lithium could transfer freely across NWO host and sulfur cathode in the discharge/charge processes, and NWO could serve as the lithium-transfer bridge to catalyze the conversion of both the solid sulfur and soluble polysulfides (Fig. 1). The certain capacity contribution of NWO in the working window would not undermine the gravimetric capacity of sulfur cathode. In the meantime, NWO possesses a good advantage of the high density up to 5.72 g cm^{-3} [38], which is beneficial to increase the tap density and volumetric capacity of sulfur-based composites. Furthermore, niobium tungsten oxides with empty d-orbitals (Lewis acid) have good adsorption and catalytic properties toward hydrogen and ethanol [39–42], signifying in potentially anchoring the electron-rich sulfur and LiPS (Lewis base) for improving the cycle stability of sulfur cathode. If this strategy is worked, the electro-active NWO would undertake good responsibility of enhancing the gravimetric and volumetric capacities, as well the cycle stability of sulfur cathode.

2. Experimental section

2.1. Preparation of NWO oxide and S/NWO composite

In a typical process, $NbCl_5$ (2.25 mmol, 99.9%, Alfa across) and WCl_6 (2 mmol, 99.9%, Alfa across) were dissolved in isopropanol (40 mL, Aladdin), and stirred for 6 h at room temperature. Then, the surfactant tetrabutylammonium hydroxide solution (TBA, 15 wt% in H_2O , Aladdin) was added into the solution, and stirred for another 12 h to

form a uniform solution. The obtained solution was transferred into a Teflon-lined stainless-steel autoclave, and heat-treated at $200 \text{ }^\circ\text{C}$ for 48 h. The precipitates were washed with water and ethanol for 3 times and dried for 12 h. The fully dried sample was sintered at $850 \text{ }^\circ\text{C}$ for 3 h in the muffle furnace.

The S/NWO composites were prepared by the chemical deposition method. $Na_2S_2O_3$ (0.04 mol) was dissolved into deionized water (400 mL) with 1 wt% polyvinylpyrrolidone. Then, the as-prepared NWO powders (0.32 g) were added into the solution and dispersed uniformly by ultrasonic treatment. Finally, dilute hydrochloric acid (0.08 mmol) was added into the solution dropwise, and nano-sized sulfur was deposited on the NWO host material. The products were collected by centrifugation at 9300 rpm for 15 min, washed with deionized water and ethanol for 6 times and dried at $60 \text{ }^\circ\text{C}$ for 12 h. The commercial carbon bp2000 was chosen as the contrast material, and the S/carbon (bp2000) composite was prepared with the same method.

2.2. Material characterization

The crystal structures of NWO oxide and S/NWO composite were studied by X-ray diffraction (XRD, Rigaku mini Flex II). The crystal structure evolutions of NWO oxide and S/NWO composite during discharge/charge process were studied by in-situ XRD (Rigaku smartlab ultra IV). The morphology of the samples was characterized with scanning electron microscopy (SEM, JEOL, JSM-7800F) and transmission electron microscopy (TEM, JEOL, JEM-2800). The sulfur contents in the composites were confirmed through thermogravimetric analysis (TG, METTLER TOLEDO, TG/DSC1). The surface areas of NWO and S/NWO samples were measured with the N_2 adsorption/desorption experiment (JW-BK112 system). The LiPS entrapment ability of the host material was evaluated by the UV–vis adsorption spectrum (Varian Cary 100 Conc UV–vis adsorption analyzer). X-ray photoelectron spectroscopy (XPS) measurements were conducted on Escalab 250Xi (Thermo Fisher Scientific).

2.3. Cell assembly and electrochemical measurement

NWO electrode, bp2000 electrode, S/NWO electrode and S/bp2000 electrode were prepared by dispersing the active material (NWO, bp2000, S/NWO, and S/bp2000), the binder poly(vinylidene fluoride) (PVdF) and the conducting agent (super P) into the N-methyl-

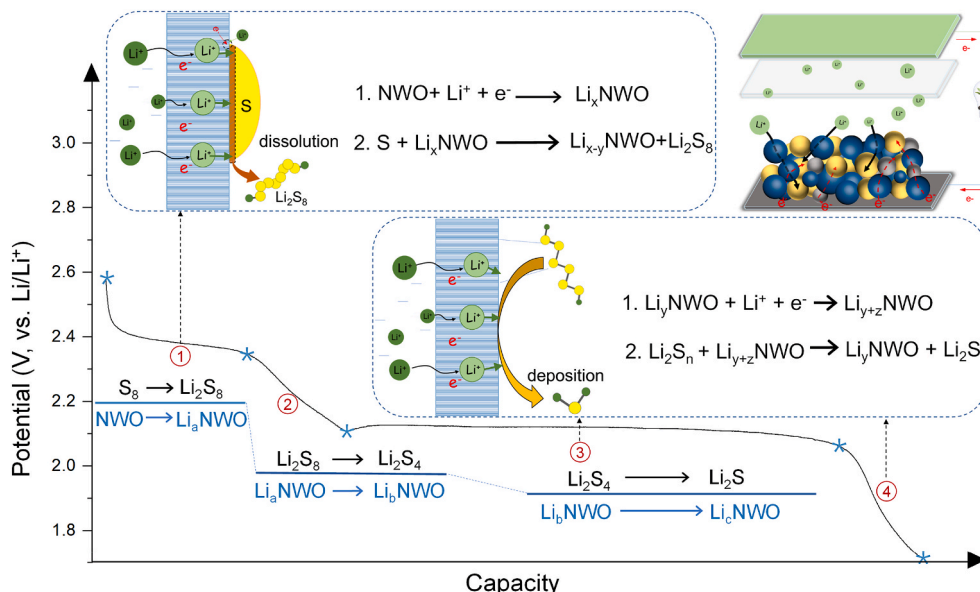


Fig. 1. Schematic illustration of the lithium-transfer bridging mechanism on niobium tungsten oxides as sulfur host.

pyrrolidone (NMP), with a mass ratio of 7:2:1. The suspension was casted onto the carbon paper (TGP-H-090) and dried at 60 °C for 48 h. Then, the cathode plate was punched into small disks with a diameter of 10 mm, and the corresponding sulfur area loading was 0.9–17 mg cm⁻². The preparation of the normal electrolyte was dissolving 1.0 M lithium bis(trifluoromethanesulphony)imide (LiTFSI) and 0.4 M LiNO₃ into the mixture of 1,3-dioxolane (DOL) and dimethyl ether (DME) with a volume ratio of 1:1. 2032-type coin cells were assembled by using Celgard 2400 as separator (18 mm), Li foil (14 mm) as anode. The electrochemical measurement was controlled in the voltage range of 1.7–2.8 V. In the in-situ XRD test, the NWO oxide was coated on the Al foil, while the S/NWO composite coated on carbon paper with the Al film to cover the window of the mould. CV measurements were performed on Chi600e workstation. The specific capacity was calculated based on sulfur as the active material, in view of the small capacity contribution of NWO.

The visual electrochemical test was implemented in an optically

transparent electrolytic cell, with the S/NWO or S/bp2000 as the cathode, Li foil (14 mm) as anode, and 5 mL normal electrolyte. Photos were taken at different depths of discharge. Linear sweep voltammetry (LSV) test and Tafel plot were conducted as following: The Li₂S₆ electrolyte (0.1 mol L⁻¹, 20 mL) used was prepared by dissolving Li₂S and S into the normal electrolyte with the molar ratio of 1:5, and stirred for 48 h at 60 °C. The three-electrode system was used, including working electrode (NWO electrode or bp2000 electrode), counter electrode (Li foil, 16 mm) and reference electrode (Li slip, 1.5 mm × 10 mm). The linear sweep of the cell was performed in the potential range of ±100 mV from the open-circuit voltage at 0.2 mV s⁻¹. The LSV measurements were performed on LK2000 workstation.

2.4. Adsorption and nucleation tests of polysulfides

Li₂S₆ solution (0.1 mol L⁻¹) was prepared by dissolving Li₂S and S into a mixture of DOL/DME solution with the mole ratio of 1:5 and

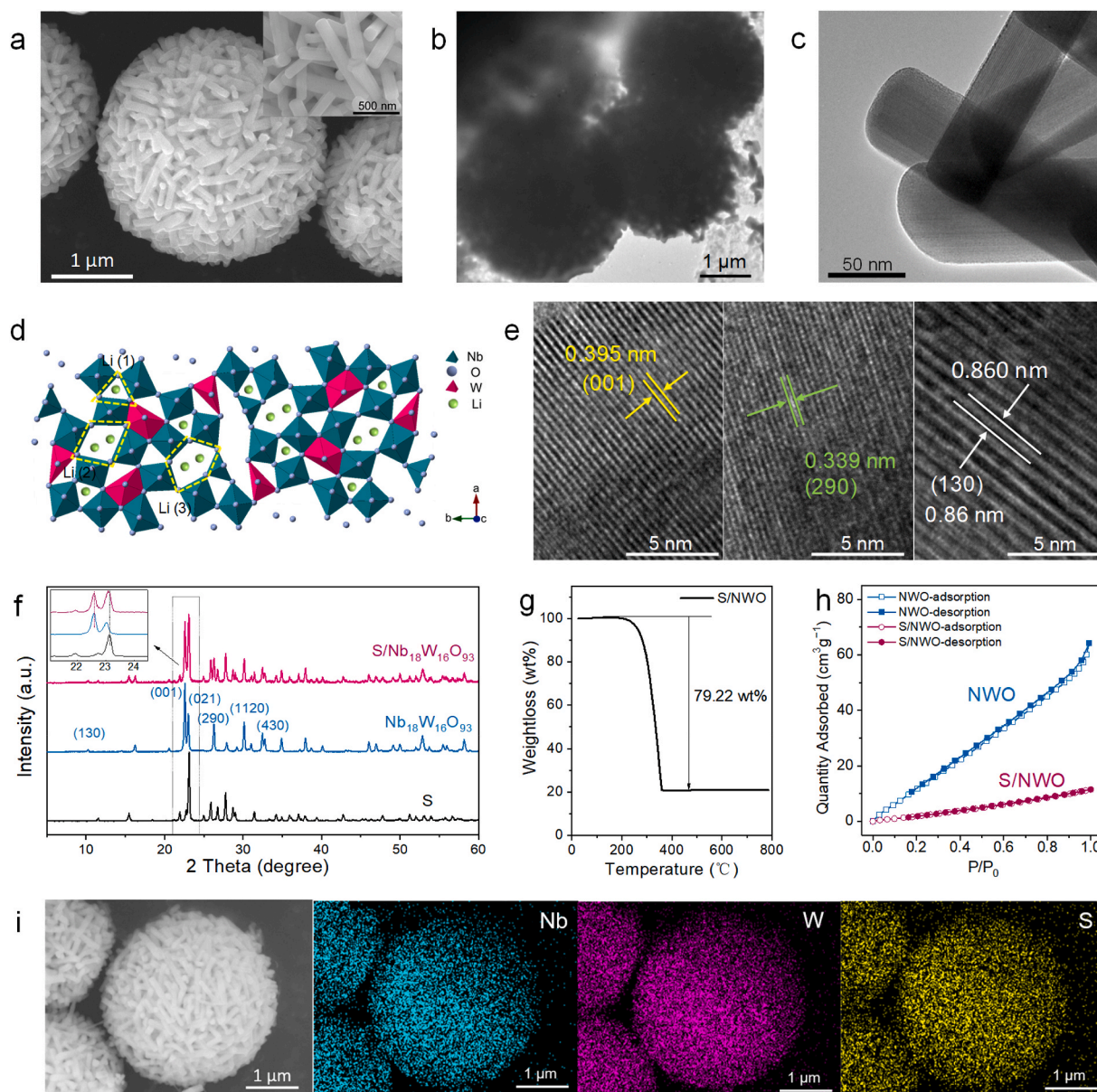


Fig. 2. Characterization of the as-prepared NWO and S/NWO composite. (a) SEM images of NWO. (b) TEM image of NWO discharged to 1.8 V. (c) TEM image of pristine NWO. (d) Schematic crystal structure of NWO. (e) HRTEM images of NWO. (f) XRD patterns of S, NWO and S/NWO composite. (g) TG curve of S/NWO composite in Ar atmosphere. (h) N₂ adsorption and desorption isotherms of NWO and S/NWO composite. (i) SEM image and EDS elemental mappings of S/NWO composite.

stirring at 60 °C for 48 h. The obtained Li_2S_6 solution was diluted to 3 and 1 mmol L^{-1} with DME before use. The NWO electrodes were beforehand discharged to 2.1 V and 1.8 V, respectively, then washed with DME and dried in the glove box. The pristine electrode, the electrode discharged to 2.1 V and 1.8 V with the same active material loading were put into Li_2S_6 solution. After standing, the liquid supernatants were taken out to test the UV-vis adsorption spectra, and the electrodes were dried for the XPS tests.

The nucleation of Li_2S was tested on the NWO and bp2000 electrodes, respectively, where the active material loading was 0.56 mg cm^{-2} . Li foil (14 mm) was chosen as the counter electrode. The adopted Li_2S_8 electrolyte (3.5 mol L^{-1}) used was prepared by dissolving Li_2S , S, LiTFSI and LiNO_3 into the tetraglyme, and stirring for 48 h at 60 °C. During the cell assembly, 5 μL normal electrolyte was dropped in the anode side and 20 μL Li_2S_8 electrolyte was dropped in the cathode side. For the nucleation test of Li_2S , the cell was first discharged galvanostatically to 2.09 V at 0.03 C and then potentiostatically discharged at 2.07 V for Li_2S nucleation for 15,000 s.

3. Results and discussion

3.1. Preparation and characterization of NWO and S/NWO composites

Niobium tungsten oxide ($\text{Nb}_{18}\text{W}_{16}\text{O}_{93}$, NWO) is prepared through a facile solvothermal and sintering process by using niobium (V) chloride and tungsten (VI) chloride as the niobium and tungsten sources, respectively (Fig. S1). With the assistance of the surfactant tetrabutylammonium (TBA, hydroxide solution), spherical precursors are prepared (Fig. S2a). After calcining at 850 °C for 3 h, porous microspheres assembled with nanorods are obtained (Fig. 2a–c and Fig. S2b). Due to the inherent small volume effect [34,35], the spherical morphology could be retained after the lithiation/delithiation reactions, which is favorable for loading sulfur into the stacking macropores/mesopores and increasing the tap density of NWO microspheres (1.86 g cm^{-3}). The prepared NWO oxide possesses typical orthorhombic structure (Pbam space group), and all the diffraction peaks are in agreement with the standard pattern (JCPDS #750-0561, Fig. 2f). HRTEM images show clear lattice spacing of 0.395, 0.339, and 0.860 nm, which match well with (001), (290) and (130) planes of bronze-like phase NWO (Fig. 2e). As shown in Fig. 2d, NWO oxide shows a typical superstructure composed of NbO_6 and WO_6 octahedra, and owns 3-, 4-, 5-sided and some S-shaped large channels along c axis, which could accommodate a large number of Li-ions and facilitate long-range diffusion of Li-ions [35].

The S/NWO composite is prepared by chemical deposition method, where the mass ratio of sulfur is 79.22 wt% (Fig. 2g). As sulfur host, NWO could still maintain the spherical morphology and orthorhombic structure in the S/NWO composite (Fig. 2f and i). It is demonstrated from EDS element mapping that Nb, W and S are distributed homogeneously among the microspheres. It illustrates that the desired loading of sulfur into the microspheres is obtained, which is further proved by the reduced surface area from 81.2 $\text{m}^2 \text{g}^{-1}$ of NWO to 14.7 $\text{m}^2 \text{g}^{-1}$ of S/NWO (Fig. 2h). In particular, the tap density of the S/NWO reaches up to 1.56 g cm^{-3} , which is far exceed the S/carbon (bp2000) composite (0.92 g cm^{-3}), under the same sulfur content (~80 wt%). Therefore, such advantages on high sulfur content, uniform distribution of sulfur, and high tap density would contribute to the desired electrochemical performance of the S/NWO composite.

3.2. Electrochemical performance

Firstly, in order to verify the electrochemical activity of NWO in the desired working window, the electrochemical properties of pure NWO oxide are studied (Fig. 3a–c). In CV curve, a pair of sharp peaks at 2.12/2.08 V (vs Li/Li^+), and the broad peaks around 1.75 V (vs Li/Li^+) can be observed (Fig. 3a), corresponding to the redox reactions of $\text{Nb}^{5+}/\text{Nb}^{4+}$

and $\text{W}^{6+}/\text{W}^{5+}$ couples [34–36], accompanied simultaneously with the lithiation/delithiation reactions. The lithiation potential is slightly lower than the conversion potential of sulfur. According to Randles-sevcik equation [30,34], CV tests with different scan rates are carried out to measure the diffusion coefficient of Li-ions (Fig. S3). The diffusion coefficients in the cathodic (reduction) and anodic (oxidation) processes are 2.08×10^{-13} and $2.28 \times 10^{-13} \text{ m}^2 \text{ s}^{-1}$, respectively, much close to that of some solid-state electrolytes [35,43]. With the fast diffusion capability of Li-ions, the prepared NWO oxide releases certain discharge capacities of 112.4, 106.8, 93.4, 82.2, and 75.5 mAh g^{-1} at 0.1, 1, 5, 10 and 20 C rate between 1.7 and 2.8 V (vs Li/Li^+), respectively, as well as good cycle stability during 300 cycles (Fig. 3b and c). Therefore, NWO is qualified as the electro-active host of sulfur, based on the certain capacity contribution and fast lithium-transfer capability in the desired working window.

The electrochemical performance of the S/NWO composite is evaluated in Li–S battery environment. In CV tests, the S/NWO composite exhibits two pairs (2.30/2.37 and 2.05/2.31 V) of typical redox peaks with higher peak currents and smaller polarization, indicating faster conversion kinetics (Fig. 3d). Meanwhile, the small peak at 2.12 V corresponds to the oxidation peak of NWO, while the reduction peak of NWO at 2.08 V is overlapped by the reduction peak of LIPS, implying a good match in the electrochemical working window. Similar to CV tests, the S/NWO composite shows smaller polarization potential (158 mV) in the discharge/charge curves. Due to the well overlapping discharge plateau of NWO and sulfur, the lithiation behavior of NWO could not be obviously observed in the CV and discharge curve of S/NWO. While the plateau corresponding to the delithiation of NWO could be observed in the early stage of charging, as shown in Fig. S4. Notably, the elevated high plateau and the extended low plateau imply a higher utilization of sulfur in the S/NWO composite (Fig. 3e), as compared with the S/carbon composite. Accordingly, the S/NWO composite releases a higher initial gravimetric capacity of 1302.6 mAh g_s^{-1} (0.1 C) than that of S/carbon composite (1130.5 mAh g_s^{-1}), with a moderate sulfur loading of ~1.5 mg cm^{-2} (Fig. 3e). Importantly, the S/NWO composite shows a great advantage on volumetric capacity (1605.3 mAh cm^{-3} composite), almost 1.9 times higher than that of the S/carbon composite (832.0 mAh cm^{-3} composite), mainly by virtue of the high tap density (1.56 g cm^{-3} vs. 0.92 g cm^{-3}). The S/NWO composite also reveals a much lower capacity decay rate as compared with the S/carbon composite (0.13% vs. 0.22% per cycle, Fig. 3g), illustrating that NWO could efficiently suppress the shuttle effect for improving the cycle stability. In addition, the S/NWO composite presents a good high-rate capability, and delivers high initial capacities of 849.0, 751.6, 634.1, 511.9 mAh g_s^{-1} at 1.0, 2.0, 5.0, 10.0 C, respectively (Fig. 3h). The capacity decay rates in long-term cycling at 1 C and 2 C can be further decreased to 0.088% and 0.083% per cycle (Fig. S5). It means that the mass transport and redox kinetics in the S/NWO electrode are fast, which may be attributed to the unique catalytic conversion ability and the as-proposed lithium-transfer bridging mechanism on NWO oxide.

Achieving the high utilization of sulfur under the high sulfur loading and low electrolyte usage is a great challenge for sulfur cathode. Herein, the S/NWO composite shows excellent electrochemical performance under the high sulfur loading and low E/S ratio (4.5 $\mu\text{L mg}^{-1}$). Under the sulfur loading of 8.3 mg cm^{-2} , the S/NWO composite could deliver a high capacity of 754.2 mAh g_s^{-1} , and show a good capacity retention of 99.5% after 130 cycles at 0.1 C (1.4 mA cm^{-2}) after activation (Fig. 3i). After increasing the sulfur loading to 10.55 mg cm^{-2} , an initial areal capacity of 8.34 mAh cm^{-2} (742.3 mAh g^{-1}) is achieved for the S/NWO electrode at 1 mA cm^{-2} (Fig. 3j). When reducing the current density to 0.13 mA cm^{-2} , the S/NWO electrode with the higher sulfur loading of 16.94 mg cm^{-2} can deliver a superhigh initial areal capacity of 19.19 mAh cm^{-2} (1132.8 mAh g^{-1}) (Fig. 3j and Fig. S6). Correspondingly, under such a high sulfur loading (16.94 mg cm^{-2}), a high gravimetric energy density of 1319.2 Wh kg^{-1} cathode of S/NWO cathode is obtained (including the binder and the conductive agent, Note S1). Therefore, by

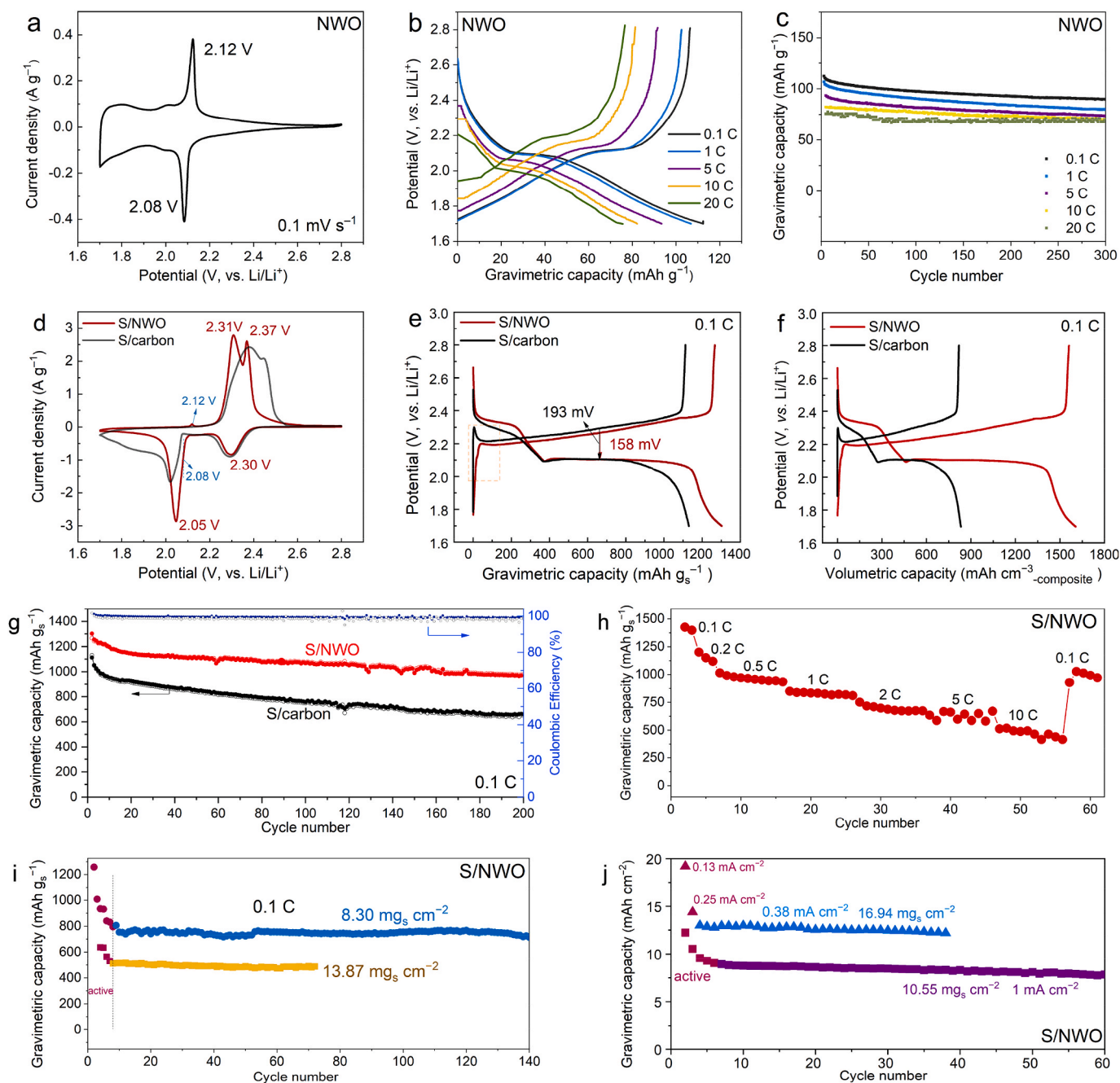


Fig. 3. Electrochemical performance of the NWO and S/NWO composite. (a) CV curve of the NWO oxide between 1.7 and 2.8 V (vs Li/Li⁺). (b) The initial discharge/charge curves and (c) the cycle performance of the NWO oxide at 0.1, 1, 5, 10 and 20 C rate between 1.7 and 2.8 V (vs Li/Li⁺) (1 C = 150 mA g⁻¹). (d) CV curves of the S/NWO and S/carbon composite at the scan rate of 0.1 mV s⁻¹. The initial discharge/charge curves of the S/NWO (1.69 mg cm⁻²) and S/carbon composite (1.53 mg cm⁻²) at 0.1C rate with the electrolyte/sulfur (E/S) ratio of 10 μ L mg⁻¹, based on (e) gravimetric calculation and (f) volumetric calculation (1 C = 1675 mA g⁻¹). (g) The cycle performance of the S/NWO composite (1.69 mg cm⁻²) and S/carbon composite (1.53 mg cm⁻²) at 0.1C rate with E/S ratio of 10 μ L mg⁻¹. (h) Rate performance of the S/NWO composite (0.95 mg cm⁻²). (i, j) The cycle performances of the S/NWO electrode with the high sulfur loadings at low E/S ratio of 4.5 μ L mg⁻¹. The electrode area is 0.785 cm² for all the electrochemical tests.

adopting the NWO host, the high utilization of sulfur could be achieved under the high sulfur loading and low electrolyte usage. In the meantime, the NWO oxide presents a desired competitive advantage as host for achieving both high gravimetric and volumetric capacities. Fig. S7 and Table S1 show the comparison on the areal capacity [8,18,44–53] and volumetric capacity [17,32,48,54–62] of this work with cathode materials for Li–S battery reported previously, further demonstrating the advantage of the electroactive NWO host on improving the electrochemical performance of the sulfur cathode. In particular, the lithium-transfer bridging mechanism on NWO oxide is working in

improving the electrochemical performance of sulfur cathode under high sulfur loading and low E/S ratio.

3.3. The interaction mechanism between lithiated NWO electrode and LiPS

Firstly, the adsorption of the pristine NWO powders is evaluated by comparing with porous carbon (bp2000). The pristine NWO powders show much stronger adsorption ability toward LiPS than porous carbon, as demonstrated by forming Nb–S [63] and W–S [64,65] bindings

(Fig. S8 and Note S2), where Nb^{5+} and W^{6+} with empty d-orbitals in NWO (Lewis acid) tend to bond with the electron-rich sulfur (Lewis bases), and induce strong chemical interaction toward LiPS [66,67]. Secondly, in consideration of the continual lithiation of NWO in the discharge process, the interaction between LiPS and different lithiated NWO (as Li_xNWO) electrodes is more important, rather than the pristine NWO. Therefore, to explore the interaction mechanism between NWO electrode and LiPS, adsorption experiments with UV-vis and XPS tests are carried out in different lithiated states (Fig. 4).

Herein, NWO electrodes discharged to 2.1 V (NWO-2.1, corresponding to Li_4NWO) and 1.8 V (NWO-1.8, corresponding to Li_{18}NWO) are chosen as the representatives of the different lithiated states. As shown in Fig. 4a, after immersion for 10 h with Li_2S_6 solution, both the NWO-2.1 and NWO-1.8 electrodes show a surprised color fading capability, as compared with the pristine NWO electrode. It illustrates that the electrochemically lithiated NWO electrodes are endowed with

stronger interaction with LiPS, such as chemical adsorption and catalytic conversion. In order to further verify the interaction mechanism of the lithiated NWO electrodes with LiPS, UV-vis and XPS tests are also conducted. As shown in UV-vis spectra (Fig. 4b), the characteristic adsorption peaks of Li_2S_6 solution are gradually decreased from NWO to NWO-2.1 and NWO-1.8 electrodes, indicating the stronger chemical interaction of the electrochemically lithiated NWO electrodes with LiPS [68–70]. More interestingly, the final product Li_2S is detected on the surface of NWO-2.1 and NWO-1.8 electrode according to the S 2p spectra (160.5 eV, Fig. 4e). It means that Li_2S_6 is completely reduced and catalytically converted to final Li_2S product by the electrochemically lithiated NWO electrodes, accompanied simultaneously with freely transferring of Li-ions from Li_xNWO to compensate charge.

Then, XPS, XRD and TEM analyses of different Li_xNWO electrodes before and after contacting with LiPS are further carried out, and the lithium-transfer bridging mechanism is proposed. As shown in XPS

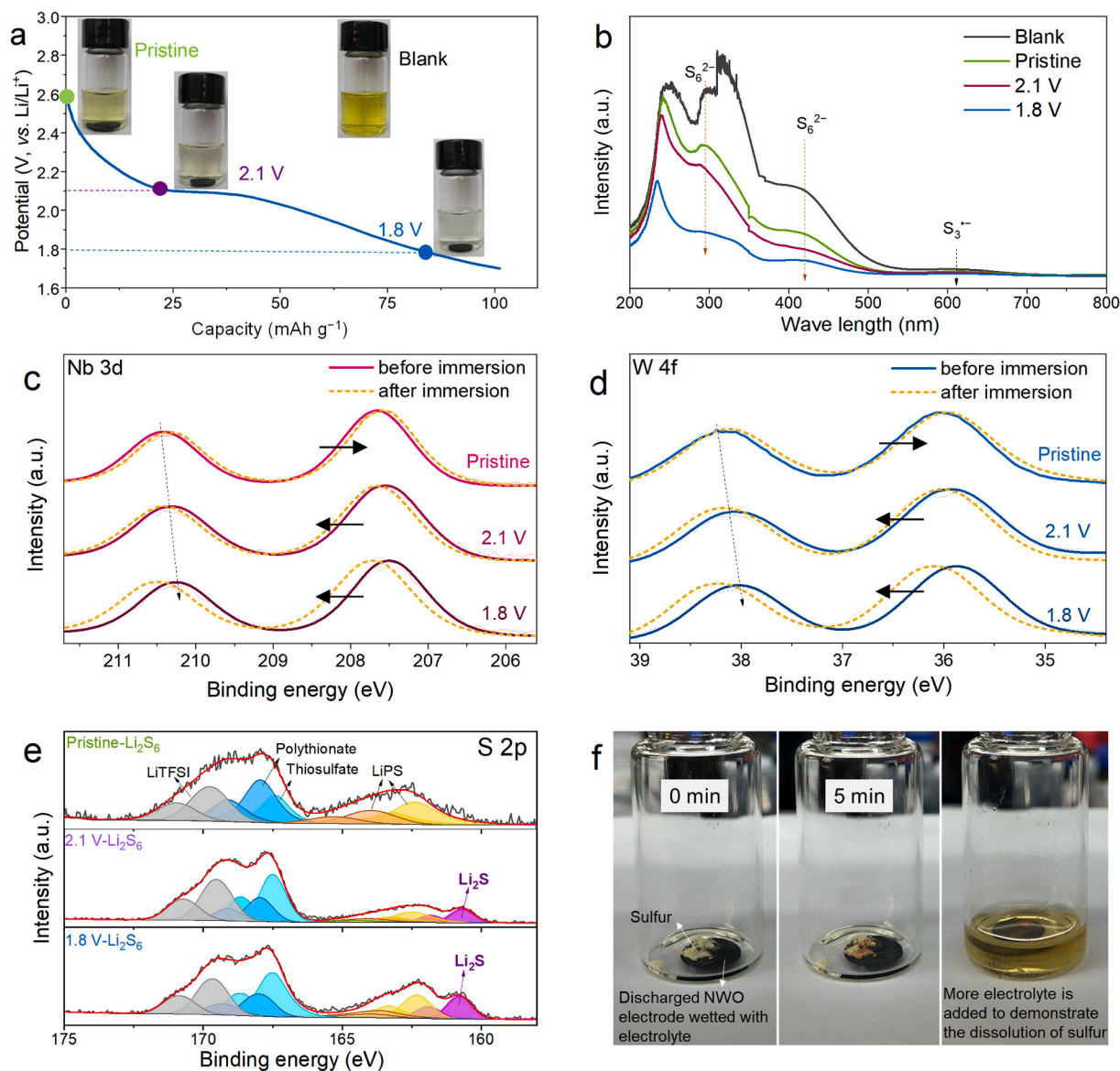


Fig. 4. (a) The discharge curve of NWO at 0.1C, and the digital photos of Li_2S_6 solutions (1 mmol L^{-1} , 5 mL) before and after contacting to the pristine NWO, NWO-2.1 and NWO-1.8 electrodes for 10 h, with the same loading (8 mg) of the active material. (b) UV-vis adsorption spectra of Li_2S_6 solution (1 mmol L^{-1} , 3 mL) before and after contacting to NWO, NWO-2.1 and NWO-1.8 electrodes for 4 h, with the same loading (5.5 mg) of the active material. XPS spectra of (c) Nb 3d, (d) W 4f and (e) S 2p on NWO, NWO-2.1 and NWO-1.8 electrodes before and after immersion with Li_2S_6 solution for 4 h. (f) The digital photos for the dissolution process of sulfur on the lithiated NWO-2.15 electrode.

spectra, the binding energy of Nb is moderately decreased from 207.65 eV (NWO) to 207.55 eV (NWO-2.1) and 207.5 eV (NWO-1.8), indicating the decreased valence state with gradual lithiation (Fig. 4c). Meanwhile, W shows an identical change tendency with Nb on the chemical state. Specifically, the binding energy of W is reduced slightly from 36.03 eV (pristine NWO) to 35.91/34.19 eV (NWO-2.1) and 35.87/34.2 eV (NWO-1.8, Fig. 4d and Fig. S9). After contacting with Li_2S_6 , the binding energies of Nb and W are moved to lower value for the pristine NWO electrode, showing the formation of Nb-S and W-S bindings, as the same with the powder sample. However, the binding energy of Nb is increased slightly from 207.55 to 207.58 eV for the NWO-2.1 electrode, and from 207.5 to 207.64 eV for the NWO-1.8 electrode, respectively, after the immersion experiment. After contacting with Li_2S_6 , the binding energy of W is shifted to higher place of 36.01/34.68 eV and 36.01/34.93 eV for the NWO-2.1 and NWO-1.8 electrodes, respectively (Fig. S9). The increased valence states of Nb and W in Li_xNWO after interacting with Li_2S_6 are different from the common valence state change caused by the Lewis acid-base interaction, and must be accompanied with the stripping of Li-ions [35]. And Li-ions/electrons are transferred from the lithiated Li_xNWO to Li_2S_6 , leading to the direct reduction of Li_2S_6 . It is a very interesting phenomenon that the lithiated Li_xNWO electrode presents the good competitive advantage over the pristine NWO to catalyze the conversion of LiPS as a Li-ions/electrons mediator, which is proposed as the lithium-transfer bridging mechanism.

To further verify the proposed interaction mechanism, XRD patterns and HRTEM images of the pristine NWO, NWO-2.1 and NWO-1.8 electrodes before and after contacting with Li_2S_6 are provided, in consideration of the crystal structure change of the oxide on the electrodes upon lithiation/delithiation. In the case of the pristine NWO electrode (Fig. 5a and Fig. S10), the anisotropic but reversible structural revolution can be observed in the discharge/charge processes. With lithiation during discharging, some lattices along *c* axis (such as (001), (021))

shrink first and then expand afterwards, which is beneficial for buffering volume expansion and maintaining structure stability during cycling [35]. While *a-b* plane lattices keep expanding after lithiation, and (1120), (390), (291) and (431) peaks are gradually shifted to the lower angles. All the peaks are recovered to the initial place after delithiation in the subsequent charge process, showing good reversibility. Therefore, it can be further judged whether there is any transportation of Li-ions between the lithiated Li_xNWO and LiPS through the lattice change in Li_xNWO . No obvious changes are observed in the crystal planes of the pristine NWO after contacting with Li_2S_6 according to XRD patterns and HRTEM images (Fig. S11). In comparison, the diffraction peaks on the immersed NWO-2.1 and NWO-1.8 electrodes are shifted to high angles (Fig. 5b), demonstrating the decrease of the interplanar spacing after contacting with Li_2S_6 . In addition, the interplanar spacing of (001) and (290) lattice of the Li_{18}NWO is decreased from 0.401 and 0.347 nm to 0.396 and 0.338 nm, respectively, on NWO-1.8 electrode after contacting with Li_2S_6 (Fig. S12). It means that the stripping of Li-ions from Li_xNWO truly occurs during the interaction with Li_2S_6 . Therefore, it is demonstrated that the Li_xNWO could facilitate the catalytic conversion of LiPS as a lithium-transfer bridge. Moreover, LiPS could be easily and directly reduced to Li_2S on the electrochemically lithiated Li_xNWO (Fig. 4e), jumping across the sluggish solid-solid conversion from Li_2S_2 to Li_2S [71]. Thus, this unique interaction on electro-active host is more effective in promoting the conversion of solid sulfur to soluble LiPS.

The conversion of solid sulfur to soluble LiPS on the lithiated Li_xNWO electrode is studied by a demonstrative experiment (Fig. 4f and Supporting videos). Firstly, the NWO electrode is discharged to 2.15 V (NWO-2.15), and then sulfur powders are putted onto the electrolyte-wetted NWO-2.15 electrode. Clearly, the yellow sulfur is turned to red after a few minutes standing, which is the color of Li_2S_8 [68]. Then, after adding more electrolyte, it seems to have the dissolution of the solid sulfur. Actually, the yellowish red electrolyte signifies the solid sulfur is

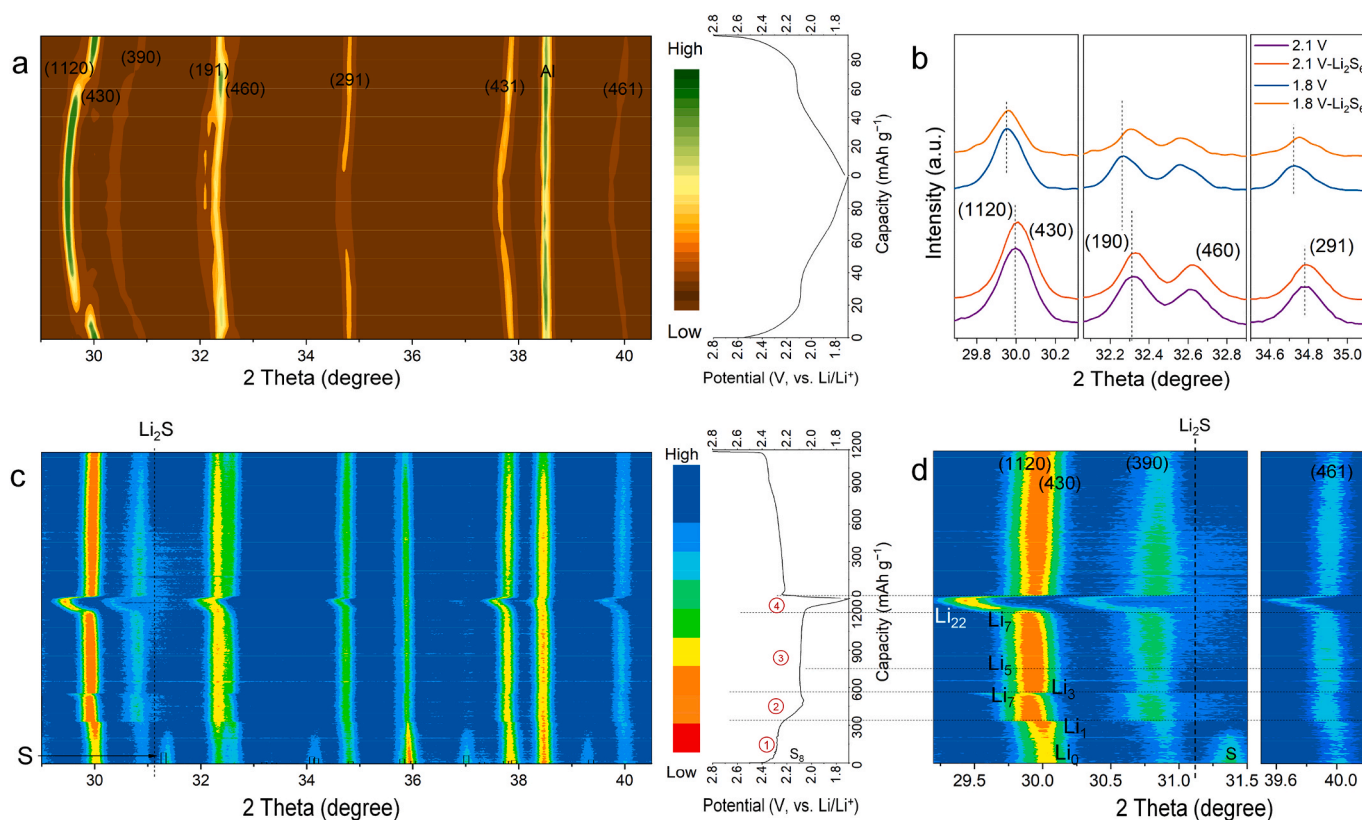


Fig. 5. (a) In-situ XRD patterns of the pristine NWO electrode in the discharge/charge processes in the potential range of 1.7–2.8 V. (b) XRD patterns of NWO-2.1 and NWO-1.8 electrodes before and after contacting with Li_2S_6 . (c,d) In-situ XRD patterns of the S/NWO electrode in the discharge/charge processes in the potential range of 1.7–2.8 V.

converted directly to Li_2S_8 by receiving Li-ions and electrons from the lithiated NWO-2.15 electrode. Of course, the pristine NWO oxide is inactive to the solid sulfur, which can guarantee the stability of the sulfur composite (Fig. S13). In addition, the interaction between Li_xNWO at different lithiated states with other soluble LiPS (Li_2S_8 and Li_2S_4) is also investigated (Fig. S14). The almost identical change tendency is obtained, and the deeper lithiated Li_xNWO could induce the more thorough color fading, illustrating the lithiated Li_xNWO could also promote the conversion of Li_2S_8 and Li_2S_4 through the as-proposed lithium-transfer bridging mechanism. Therefore, the conversion from the solid sulfur to soluble LiPS, and the final solid Li_2S can be accelerated by the lithium-transfer bridging mechanism on electro-active NWO host (Fig. 1). As shown in the cathodic reaction ($\text{S} + 2\text{Li}^+ + 2\text{e}^- = \text{Li}_2\text{S}_x$, $1 < x < 8$), sulfur species, Li-ions, and electrons are three indispensable factors in the cathode conversion. As the absorber of LiPS and transporter of Li-ions/electrons, the electrochemically lithiated Li_xNWO is highly efficient in accelerating the redox reaction of sulfur cathode.

Supplementary video related to this article can be found at <https://doi.org/10.1016/j.nanoen.2020.105173>

The function of NWO oxides in Li-S battery system is further explored by in-situ XRD measurement. Based on the reaction mechanism and in-situ XRD results, the discharge process can be tentatively divided into four stages (Fig. 6 and Fig. S15) [72]. In the first stage, solid sulfur is reduced to liquid Li_2S_8 , which is dissolved in the electrolyte. As to the sulfur cathode with conventional hosts, the transferring of Li-ions to active material (sulfur) happens only from liquid electrolyte on the solid/liquid interface. When the NWO is used as electro-active hosts, the in-situ electrochemically lithiated Li_xNWO could serve as the conductor of Li-ions/electrons, providing two transfer paths of Li-ions on the

solid/solid (S/ Li_xNWO) and solid/liquid (S/electrolyte) interfaces. It means that the utilization of the insulating sulfur on the solid/solid (S/ Li_xNWO) interface can be increased, as demonstrated by the completely disappeared peaks of the orthorhombic S_8 (Fig. 5c and d and Fig. 6b and c). Meanwhile, the characteristic peaks of NWO are slowly moved to lower angles (NWO to Li_1NWO , the number of Li-ions is roughly calculated, Note S3). In the second stage, liquid Li_2S_8 is further reduced to short-chain Li_2S_6 and Li_2S_4 , existing in electrolyte. The number of soluble LiPS and the viscosity of electrolyte reach the maximum, where the shuttling is easy to occur without effective host [73]. Interestingly, along with the potential sudden drop, the diffraction peaks of NWO are rapidly shifted to lower angles with lithiation by forming Li_7NWO , then re-shifted back to high angles (Li_3NWO) at the beginning of the second discharge plateau (Fig. 5d). It is confirmed that the transferring of Li-ions occurs from the lithiated Li_xNWO to LiPS on the solid/liquid interface. Furthermore, the strong interaction of Li_xNWO and LiPS could result in the formation of Li_2S on the interface with the newly emerged peaks at 27.03° , 31.31° and 44.88° (Fig. S15). However, the Li_2S formed on the interface disappears quickly under the high-concentrated LiPS environment due to the following reaction: $2/5 \text{Li}_2\text{S} + 3/5 \text{S}_6^{2-} = \text{S}_4^{2-} + 4/5 \text{Li}^+$ [74], and would insure the clean and active surface of the NWO host for the subsequent reactions. The third stage is the two-phase reduction process with a flat and long plateau region from soluble Li_2S_4 to insoluble Li_2S . The lithiation/delithiation processes of $\text{Li}_{5+x}\text{NWO}$ are repeated smoothly, exhibiting the almost unchanged diffraction peak of the host in the third stage (Fig. 5c and d and Fig. 6). Herein, $\text{Li}_{5+x}\text{NWO}$ could transfer Li-ions/electrons for trapping LiPS, leading to the rapid reduction of LiPS. Usually, in the last stage, some residual LiPS are still observed from the yellow separator in

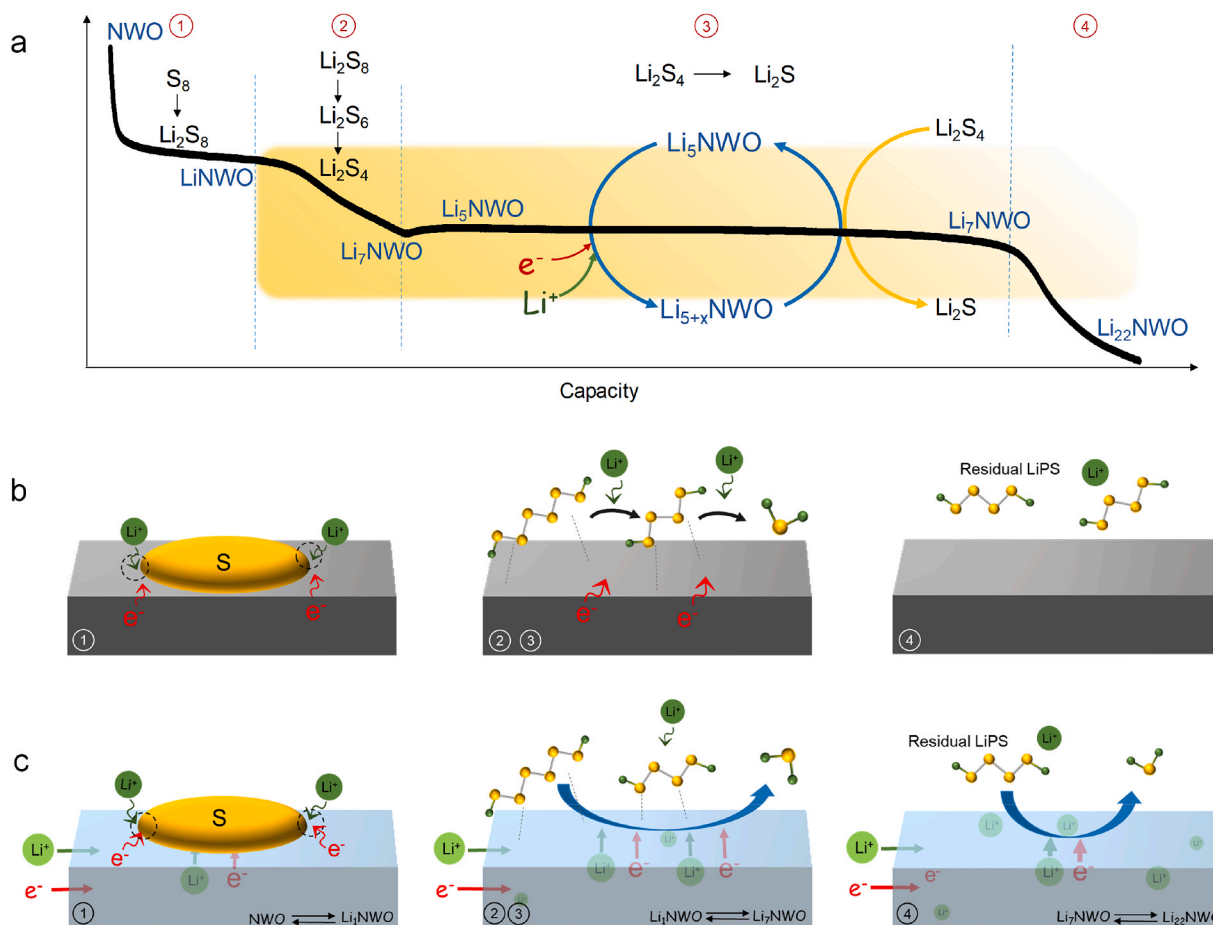


Fig. 6. (a) Scheme of the interaction of NWO and lithiated Li_xNWO with the sulfur species in the different discharge stages of the sulfur cathode. Schematic illustration of the working mechanism of the (b) conventional host, and (c) electro-active NWO host in Li-S battery.

S/carbon cell (Fig. S17a). While the lithiated Li_xNWO is highly efficient for converting the residual LiPS, as verified by the nearly colorlessly separator in the discharged cell (Fig. S17b). Therefore, the NWO is in-situ electrochemically lithiated as Li_xNWO in the discharge process, which plays a positive role in all the conversion stages of sulfur during discharging by the lithium-transfer bridging mechanism. Such an interaction mechanism with the strong entrapment and catalytic conversion of LiPS can be verified by the visual electrochemical test in the optically transparent cells (Fig. S18).

3.4. Electrochemical kinetics

Herein, the electrochemical kinetics of soluble LiPS is the key issue, which is evaluated on the NWO oxide, including the conversion from liquid long-chain LiPS to liquid short-chain LiPS, and from liquid short-chain LiPS to final solid Li_2S product. As shown in linear sweep voltammetry (LSV, Fig. S19) and corresponding Tafel plots (Fig. S20), the reduction onset potential of Li_2S_6 on NWO (2.319 V) is higher, indicating the easier reduction of Li_2S_6 . In particular, the higher exchange current density (0.12 mA cm^{-2} vs. 0.10 mA cm^{-2}) represents a greatly enhanced conversion rate of long-chain LiPS on NWO. In the oxidation process, the lower onset potential (2.363 V) and higher exchange current density (0.16 mA cm^{-2}) are observed, verifying the fast oxidation kinetics of Li_2S_6 under the efficient catalysis of NWO.

The effective deposition of final solid Li_2S is another critical step in the electrochemical process. The electrochemical deposition of Li_2S on NWO and carbon hosts are compared with the potentiostatic discharge tests. The galvanostatic intermittent titration experiments (GITT) are implemented to obtain the equilibrium potential, which is $\sim 2.17 \text{ V}$ for both cells, thus the potential for potentiostatic discharge is accordingly set at 2.07 V (Fig. S21) [75]. It is found from the current-time curves that the Li_2S nucleation is earlier on NWO oxide with a higher capacity of 201.9 mAh g^{-1} , as compared with porous carbon (123.0 mAh g^{-1} , Fig. S22). It means that the conversion and deposition from soluble LiPS to solid Li_2S are more effective and adequate on NWO.

4. Conclusions

In high energy density Li-S battery, the effective anchoring of sulfur/LiPS, and the timely transfer of Li-ions/electrons are necessary to ensure the high sulfur utilization in the electrochemical reaction, especially in the thick and dense electrode with lean electrolyte. In this work, the NWO microspheres are chosen as the electroactive host of sulfur for fabricating sulfur cathode. Herein, the NWO microspheres show the strong chemical adsorption toward LiPS, the certain capacity contribution, and fast lithium-transfer capability in the desired working window. Especially, the in-situ electrochemically lithiated Li_xNWO serves as good electrocatalyst and lithium-transfer bridge to facilitate the effective conversion of both sulfur and LiPS to final Li_2S product, and significantly improves the sulfur utilization under high sulfur content, high sulfur loading and lean electrolyte condition. Specifically, the S/NWO electrode delivers a high areal capacity ($19.19 \text{ mAh cm}^{-2}$) under both high sulfur loading (16.94 mg cm^{-2}) and low electrolyte/sulfur ratio ($4.5 \mu\text{L mg}^{-1}$). Meanwhile, due to the high tap density (1.56 g cm^{-3}), the S/NWO composite presents a great advantage on volumetric capacity ($1605.3 \text{ mAh cm}^{-3}_{\text{composite}}$), almost 1.9 times higher than that of the S/carbon composite ($832.0 \text{ mAh cm}^{-3}_{\text{composite}}$). This work also provides a new understanding by using the electroactive host of sulfur in achieving high energy Li-S battery.

Declaration of competing interest

The authors declare that they have no known competing financial interests or personal relationships that could have appeared to influence the work reported in this paper.

CRedit authorship contribution statement

Lu Wang: Conceptualization, Investigation, Writing - original draft. **Zhen-Yu Wang:** Methodology. **Jun-Feng Wu:** Methodology. **Guo-Ran Li:** Formal analysis. **Sheng Liu:** Formal analysis. **Xue-Ping Gao:** Conceptualization, Resources, Writing - review & editing, Supervision.

Acknowledgements

Financial support from the National Key Research and Development Program (2016YFB0100200), and National Natural Science Foundation of China (21935006 and 21421001) of China is gratefully acknowledged.

Appendix A. Supplementary data

Supplementary data to this article can be found online at <https://doi.org/10.1016/j.nanoen.2020.105173>.

References

- [1] J.W. Choi, D. Aurbach, Promise and reality of post-lithium-ion batteries with high energy densities, *Nat. Rev. Mater.* 1 (2016) 16013.
- [2] Z.P. Cano, D. Banham, S.Y. Ye, A. Hintennach, J. Lu, M. Fowler, Z.W. Chen, Batteries and fuel cells for emerging electric vehicle markets, *Nat. Energy* 3 (2018) 279–289.
- [3] H.T. Sun, J. Zhu, D. Baumann, L.L. Peng, Y.X. Xu, I. Shakir, Y. Huang, X.F. Duan, Hierarchical 3D electrodes for electrochemical energy storage, *Nat. Rev. Mater.* 4 (2018) 45–60.
- [4] Q. Pang, X. Liang, C.Y. Kwok, L.F. Nazar, Advances in lithium-sulfur batteries based on multifunctional cathodes and electrolytes, *Nat. Energy* 1 (2016) 16132.
- [5] J.N. Wang, G.R. Yang, J. Chen, Y.P. Liu, Y.K. Wang, C.Y. Lao, K. Xi, D.W. Yang, C. J. Harris, W. Yan, S.J. Ding, R.V. Kumar, Flexible and high-loading lithium-sulfur batteries enabled by integrated three-in-one fibrous membranes, *Adv. Energy Mater.* 9 (2019), 1902001.
- [6] L.L. Kong, L. Wang, Z.C. Ni, S. Liu, G.R. Li, X.P. Gao, Lithium-magnesium alloy as a stable anode for lithium-sulfur battery, *Adv. Funct. Mater.* 29 (2019), 1808756.
- [7] Z.Y. Wang, L. Wang, S. Liu, G.R. Li, X.P. Gao, Conductive CoOOH as carbon-free sulfur immobilizer to fabricate sulfur-based composite for lithium-sulfur battery, *Adv. Funct. Mater.* 29 (2019), 1901051.
- [8] Q. Pang, D. Kundu, L.F. Nazar, A graphene-like metallic cathode host for long-life and high-loading lithium-sulfur batteries, *Mater. Horiz.* 3 (2016) 130–136.
- [9] W.L. Cai, G.R. Li, K.L. Zhang, G.N. Xiao, C. Wang, K.F. Ye, Z.W. Chen, Y.C. Zhu, Y. T. Qian, Conductive nanocrystalline niobium carbide as high-efficiency polysulfides tamer for lithium-sulfur batteries, *Adv. Funct. Mater.* 28 (2018), 1704865.
- [10] Y. Hu, W. Chen, T.Y. Lei, B. Zhou, Y. Jiao, Y.C. Yan, X.C. Du, J.W. Huang, C.Y. Wu, X.P. Wang, Y. Wang, B. Chen, J. Xu, C. Wang, J. Xiong, Carbon quantum dots-modified interfacial interactions and ion conductivity for enhanced high current density performance in lithium-sulfur batteries, *Adv. Energy Mater.* 9 (2019), 1802955.
- [11] M. Yan, H. Chen, Y. Yu, H. Zhao, C.F. Li, Z.Y. Hu, P. Wu, L.H. Chen, H.G. Wang, D. L. Peng, H.X. Gao, T. Hasan, Y. Li, B.L. Su, 3D ferroconcrete-like aminated carbon nanotubes network anchoring sulfur for advanced lithium-sulfur battery, *Adv. Energy Mater.* 8 (2018), 1801066.
- [12] H. Zhang, W.Q. Zhao, M.C. Zou, Y.S. Wang, Y.J. Chen, L. Xu, H.S. Wu, A.Y. Cao, 3D, mutually embedded MOF@carbon nanotube hybrid networks for high-performance lithium-sulfur batteries, *Adv. Energy Mater.* 8 (2018), 1800013.
- [13] Z.Y. Wang, Y.F. Dong, H.J. Li, Z.B. Zhao, H.B. Wu, C. Hao, S.H. Liu, J.S. Qiu, X. W. Lou, Enhancing lithium-sulphur battery performance by strongly binding the discharge products on amino-functionalized reduced graphene oxide, *Nat. Commun.* 5 (2014) 5002.
- [14] Z. Zhang, L.L. Kong, S. Liu, G.R. Li, X.P. Gao, A high-efficiency sulfur/carbon composite based on 3D graphene nanosheet@carbon nanotube matrix as cathode for lithium-sulfur battery, *Adv. Energy Mater.* 7 (2017), 1602543.
- [15] L.L. Kong, Z. Zhang, Y.Z. Zhang, S. Liu, G.R. Li, X.P. Gao, Porous carbon paper as interlayer to stabilize the lithium anode for lithium-sulfur battery, *ACS Appl. Mater. Interfaces* 8 (2016) 31684–31694.
- [16] D.W. Su, M. Cortie, G.X. Wang, Fabrication of N-doped graphene-carbon nanotube hybrids from prussian blue for lithium-sulfur batteries, *Adv. Energy Mater.* 7 (2017), 1602014.
- [17] Z. Zhang, D.H. Wu, Z. Zhou, G.R. Li, S. Liu, X.P. Gao, Sulfur/nickel ferrite composite as cathode with high-volumetric-capacity for lithium-sulfur battery, *Sci. China Mater.* 62 (2019) 74–86.
- [18] Q. Pang, C.Y. Kwok, D. Kundu, X. Liang, L.F. Nazar, Lightweight metallic MgB_2 mediates polysulfide redox and promises high-energy-density lithium-sulfur batteries, *Joule* 3 (2019) 136–148.
- [19] W.J. Xue, Z. Shi, L.M. Suo, C. Wang, Z.Q. Wang, H.Z. Wang, K.P. So, A. Maurano, D.W. Yu, Y.M. Chen, L. Qie, Z. Zhu, G.Y. Xu, J. Kong, J. Li, Intercalation-conversion

- hybrid cathodes enabling Li-S full-cell architectures with jointly superior gravimetric and volumetric energy densities, *Nat. Energy* 4 (2019) 374–382.
- [20] Y.T. Liu, D.D. Han, L. Wang, G.R. Li, S. Liu, X.P. Gao, NiCo₂O₄ nanofibers as carbon-free sulfur immobilizer to fabricate sulfur-based composite with high volumetric capacity for lithium-sulfur battery, *Adv. Energy Mater.* 9 (2019), 1803477.
- [21] L. Wang, B.H. Zhang, Y.T. Liu, Z.Y. Wang, G.R. Li, S. Liu, X.P. Gao, Spherical metal oxides with high tap density as sulfur host to enhance cathode volumetric capacity for lithium-sulfur battery, *ACS Appl. Mater. Interfaces* 12 (2020) 5909–5919.
- [22] B. Zhang, C.H. Xiao, S.M. Xie, J. Liang, X. Chen, Y.H. Tang, Iron-nickel nitride nanostructures in situ grown on surface-redox-etching nickel foam: efficient and ultrasustainable electrocatalysts for overall water splitting, *Chem. Mater.* 28 (2016) 6934–6941.
- [23] Z.M. Cui, C.X. Zu, W.D. Zhou, A. Manthiram, J.B. Goodenough, Mesoporous titanium nitride-enabled highly stable lithium-sulfur batteries, *Adv. Mater.* 28 (2016) 6926–6931.
- [24] Z.H. Sun, J.Q. Zhang, L.C. Yin, G.J. Hu, R.P. Fang, H.M. Cheng, F. Li, Conductive porous vanadium nitride/graphene composite as chemical anchor of polysulfides for lithium-sulfur batteries, *Nat. Commun.* 8 (2017) 14627.
- [25] X.C. Gao, D. Zhou, Y. Chen, W.J. Wu, D.W. Su, B.H. Li, G.X. Wang, Strong charge polarization effect enabled by surface oxidized titanium nitride for lithium-sulfur batteries, *Commun. Chem.* 2 (2019) 1–10.
- [26] X. Liu, J.Q. Huang, Q. Zhang, L.Q. Mai, Nanostructured metal oxides and sulfides for lithium-sulfur batteries, *Adv. Mater.* 29 (2017), 1601759.
- [27] J. Xu, W.X. Zhang, H.B. Fan, F.L. Cheng, D.W. Su, G.X. Wang, Promoting lithium polysulfide/sulfide redox kinetics by the catalyzing of zinc sulfide for high performance lithium-sulfur battery, *Nano Energy* 51 (2018) 73–82.
- [28] H.H. Xu, A. Manthiram, Hollow cobalt sulfide polyhedra-enabled long-life, high areal-capacity lithium-sulfur batteries, *Nano Energy* 33 (2017) 124–129.
- [29] H.T. Wang, Q.F. Zhang, H.B. Yao, Z. Liang, H.W. Lee, P.C. Hsu, G.Y. Zheng, Y. Cui, High electrochemical selectivity of edge versus terrace sites in two-dimensional layered MoS₂ materials, *Nano Lett.* 14 (2014) 7138–7144.
- [30] G.M. Zhou, H.Z. Tian, Y. Jin, X.Y. Tao, B.F. Liu, R.F. Zhang, Z.W. Seh, D. Zhuo, Y. Y. Liu, J. Sun, J. Zhao, C.X. Zu, D.S.C. Wu, Q.F. Zhang, Y. Cui, Catalytic oxidation of Li₂S on the surface of metal sulfides for Li-S batteries, *Proc. Natl. Acad. Sci. U.S.A.* 114 (2017) 840–845.
- [31] Y.T. Liu, S. Liu, G.R. Li, T.Y. Yan, X.P. Gao, High volumetric energy density sulfur cathode with heavy and catalytic metal oxide host for lithium-sulfur battery, *Adv. Sci.* 7 (2020), 1903693.
- [32] Z.Y. Wang, D.D. Han, S. Liu, G.R. Li, T.Y. Yan, X.P. Gao, Conductive RuO₂ stacking microspheres as an effective sulfur immobilizer for lithium-sulfur battery, *Electrochim. Acta* 337 (2020), 135772.
- [33] S.H. Choi, D.W. Su, M. Shin, S. Park, G.X. Wang, Pomegranate-structured silica/sulfur composite cathodes for high performance lithium-sulfur batteries, *Chem. Asian J.* 13 (2018) 568–576.
- [34] W.Q. Ye, H.X. Yu, X. Cheng, H.J. Zhu, R.T. Zheng, T.T. Liu, N.B. Long, M. Shui, J. Shu, Highly efficient lithium container based on non-Wadsley-Roth structure Nb₁₈W₁₆O₉₃ nanowires for electrochemical energy storage, *Electrochim. Acta* 292 (2018) 331–338.
- [35] K.J. Griffith, K.M. Wiaderek, G. Cibir, L.E. Marbella, C.P. Grey, Niobium tungsten oxides for high-rate lithium-ion energy storage, *Nature* 559 (2018) 556–563.
- [36] L. Yan, J. Shu, C.X. Li, X. Cheng, H.J. Zhu, H.X. Yu, C.F. Zhang, Y. Zheng, Y. Xie, Z. P. Guo, W₃Nb₁₄O₄₄ nanowires: ultrastable lithium storage anode materials for advanced rechargeable batteries, *Energy Storage Mater.* 16 (2019) 535–544.
- [37] L. Yan, X. Cheng, H.X. Yu, H.J. Zhu, T.T. Liu, R.T. Zheng, R.F. Zhang, M. Shui, J. Shu, Ultrathin W₉Nb₈O₄₇ nanofibers modified with thermal NH₃ for superior electrochemical energy storage, *Energy Storage Mater.* 14 (2018) 159–168.
- [38] N.C. Stephenson, A structural investigation of some stable phases in the region Nb₂O₅-WO₃-WO₃, *Acta Crystallogr.* 24 (1968) 637–653.
- [39] J. Yu, H. Wen, M. Shafiei, M.R. Field, Z.F. Liu, W. Wlodarski, N. Motta, Y.X. Li, K. Kalantar-zadeh, P.T. Lai, A hydrogen/methane sensor based on niobium tungsten oxide nanorods synthesised by hydrothermal method, *Sens. Actuators, B* 184 (2013) 118–129.
- [40] C. Tagusagawa, A. Takagaki, A. Iguchi, K. Takanabe, J.N. Kondo, K. Ebitani, S. Hayashi, T. Tatsumi, K. Domen, Highly active mesoporous Nb-W oxide solid-acid catalyst, *Angew. Chem. Int. Ed.* 49 (2010) 1128–1132.
- [41] C.C. Yue, X.C. Zhu, M. Rigutto, E. Hensen, Acid catalytic properties of reduced tungsten and niobium-tungsten oxides, *Appl. Catal., B* 163 (2015) 370–381.
- [42] R. Liu, J.J. Lin, L.Y. Chou, S.W. Sheehan, W.S. He, F. Zhang, H.J.M. Hou, D. W. Wang, Water splitting by tungsten oxide prepared by atomic layer deposition and decorated with an oxygen-evolving catalyst, *Angew. Chem. Int. Ed.* 50 (2011) 499–502.
- [43] K. Hayamizu, S. Seki, Long-range Li ion diffusion in NASICON-type Li_{1.5}Al_{0.5}Ge_{1.5}(PO₄)₃ (LAGP) studied by ⁷Li pulsed-gradient spin-echo NMR, *Phys. Chem. Chem. Phys.* 19 (2017) 23483–23491.
- [44] Y. Chen, W.X. Zhang, D. Zhou, H.J. Tian, D.W. Su, C.Y. Wang, D. Stockdale, F. Y. Kang, B.H. Li, G.X. Wang, Co-Fe mixed metal phosphide nanocubes with highly interconnected-pore architecture as an efficient polysulfide mediator for lithium-sulfur batteries, *ACS Nano* 13 (2019) 4731–4741.
- [45] Y. Chen, S. Choi, D.W. Su, X.C. Gao, G.X. Wang, Self-standing sulfur cathodes enabled by 3D hierarchically porous titanium monoxide-graphene composite film for high-performance lithium-sulfur batteries, *Nano Energy* 47 (2018) 331–339.
- [46] Y.J. Li, J.B. Wu, B. Zhang, W.Y. Wang, G.Q. Zhang, Z.W. Seh, N. Zhang, J. Sun, L. Huang, J.J. Jiang, J. Zhou, Y.M. Sun, Fast conversion and controlled deposition of lithium (poly)sulfides in lithium-sulfur batteries using high-loading cobalt single atoms, *Energy Storage Mater.* 30 (2020) 250.
- [47] Y.J. Li, C. Wang, W.Y. Wang, A.Y.S. Eng, M.T. Wan, L. Fu, E. Mao, G.C. Li, J. Tang, Z.W. Seh, Y.M. Sun, Enhanced chemical immobilization and catalytic conversion of polysulfide intermediates using metallic Mo nanoclusters for high-performance Li-S batteries, *ACS Nano* 14 (2020) 1148–1157.
- [48] Y.Y. Mao, G.R. Li, Y. Guo, Z.P. Li, C.D. Liang, X.S. Peng, Z. Lin, Foldable interpenetrated metal-organic frameworks/carbon nanotubes thin film for lithium-sulfur batteries, *Nat. Commun.* 8 (2017) 14628.
- [49] L. Luo, S.H. Chung, A. Manthiram, Rational design of a dual-function hybrid cathode substrate for lithium-sulfur batteries, *Adv. Energy Mater.* 8 (2018), 1801014.
- [50] Y. Wang, R. Zhang, J. Chen, H. Wu, S. Lu, K. Wang, H. Li, C.J. Harris, K. Xi, R. V. Kumar, S. Ding, Enhancing catalytic activity of titanium oxide in lithium-sulfur batteries by band engineering, *Adv. Energy Mater.* 9 (2019), 1900953.
- [51] J. Wang, G. Yang, J. Chen, Y. Liu, Y. Wang, C.Y. Lao, K. Xi, D. Yang, C.J. Harris, W. Yan, S. Ding, R.V. Kumar, Flexible and high-loading lithium-sulfur batteries enabled by integrated three-in-one fibrous membranes, *Adv. Energy Mater.* 9 (2019), 1902001.
- [52] Y. Yang, Y. Zhong, Q. Shi, Z. Wang, K. Sun, H. Wang, Electrocatalysis in lithium sulfur batteries under lean electrolyte conditions, *Angew. Chem. Int. Ed.* 57 (2018) 15549–15552.
- [53] J. He, L. Luo, Y. Chen, A. Manthiram, Yolk-shelled C@Fe₃O₄ nanoboxes as efficient sulfur hosts for high-performance lithium-sulfur batteries, *Adv. Mater.* 29 (2017), 1702707.
- [54] X.B. Cheng, J.Q. Huang, Q. Zhang, H.J. Peng, M.Q. Zhao, F. Wei, Aligned carbon nanotube/sulfur composite cathodes with high sulfur content for lithium-sulfur batteries, *Nano Energy* 4 (2014) 65–72.
- [55] M. Li, Y.N. Zhang, F. Hassan, W. Ahn, X.L. Wang, W.W. Liu, G.P. Jiang, Z.W. Chen, Compact high volumetric and areal capacity lithium sulfur batteries through rock salt induced nano-architected sulfur hosts, *J. Mater. Chem. A* 5 (2017) 21435–21441.
- [56] H. Li, Y. Tao, C. Zhang, D.H. Liu, J.Y. Luo, W.C. Fan, Y. Xu, Y.Z. Li, C.H. You, Z. Z. Pan, M.C. Ye, Z.Y. Chen, Z. Dong, D.W. Wang, F.Y. Kang, J. Lu, Q.H. Yang, Dense graphene monolith for high volumetric energy density Li-S batteries, *Adv. Energy Mater.* 8 (2018), 1703438.
- [57] Z.L. Li, Z.B. Xiao, S.Q. Wang, Z.B. Cheng, P.Y. Li, R.H. Wang, Engineered interdiffusion of hollow nitrogen-doped carbon nanospheres for improving electrochemical behavior and energy density of lithium-sulfur batteries, *Adv. Funct. Mater.* 29 (2019), 1902322.
- [58] P.T. Xiao, F.X. Bu, G.H. Yang, Y. Zhang, Y. Xu, Integration of graphene, nano sulfur, and conducting polymer into compact, flexible lithium-sulfur battery cathodes with ultrahigh volumetric capacity and superior cycling stability for foldable devices, *Adv. Mater.* 29 (2017), 1703324.
- [59] F. Pei, L.L. Lin, D.H. Ou, Z.M. Zheng, S.G. Mo, X.L. Fang, N.F. Zheng, Self-supporting sulfur cathodes enabled by two-dimensional carbon yolk-shell nanosheets for high-energy-density lithium-sulfur batteries, *Nat. Commun.* 8 (2017) 482.
- [60] K. Xi, D.Q. He, C. Harris, Y.K. Wang, C. Lai, H.L. Li, P.R. Coxon, S.J. Ding, C. Wang, R.V. Kumar, Enhanced sulfur transformation by multifunctional FeS₂/FeS/S composites for high-volumetric capacity cathodes in lithium-sulfur batteries, *Adv. Sci.* 6 (2019), 1800815.
- [61] J.X. Song, M.L. Gordin, T. Xu, S.R. Chen, Z.X. Yu, H. Sohn, J. Lu, Y. Ren, Y.H. Duan, D.H. Wang, Strong lithium polysulfide chemisorption on electroactive sites of nitrogen-doped carbon composites for high-performance lithium-sulfur battery cathodes, *Angew. Chem. Int. Ed.* 54 (2015) 4399–4403.
- [62] H.F. Li, X.W. Yang, X.M. Wang, M.N. Liu, F.M. Ye, J. Wang, Y.C. Qiu, W.F. Li, Y. G. Zhang, Dense integration of graphene and sulfur through the soft approach for compact lithium/sulfur battery cathode, *Nano Energy* 12 (2015) 468–475.
- [63] X.X. Li, B. Gao, X. Huang, Z.J. Guo, Q.W. Li, X.M. Zhang, P.K. Chu, K.F. Huo, Conductive mesoporous niobium nitride microspheres/nitrogen-doped graphene hybrid with efficient polysulfide anchoring and catalytic conversion for high-performance lithium-sulfur batteries, *ACS Appl. Mater. Interfaces* 11 (2019) 2961–2969.
- [64] B. Zhang, C. Luo, Y. Deng, Z. Huang, G. Zhou, W. Lv, Y.B. He, Y. Wan, F. Kang, Q. H. Yang, Optimized catalytic WS₂-WO₃ heterostructure design for accelerated polysulfide conversion in lithium-sulfur batteries, *Adv. Energy Mater.* 10 (2020), 2000091.
- [65] S. Choi, D.H. Seo, M.R. Kaiser, C.M. Zhang, T. van der laan, Z.J. Han, A. Bendavid, X. Guo, S. Yick, A.T. Murdock, D. Su, B.R. Lee, A. Du, S.X. Dou, G.X. Wang, WO₃ nanolayer coated 3D-graphene/sulfur composites for high performance lithium/sulfur batteries, *J. Mater. Chem. A* 7 (2019) 4596–4603.
- [66] D. Su, M. Cortie, H.B. Fan, G.X. Wang, Prussian blue nanocubes with an open framework structure coated with PEDOT as high-capacity cathodes for lithium-sulfur batteries, *Adv. Mater.* 29 (2017), 1700587.
- [67] Q. Pang, X. Liang, C.Y. Kwok, L.F. Nazar, Advances in lithium-sulfur batteries based on multifunctional cathodes and electrolytes, *Nat. Energy* 1 (2016) 1–11.
- [68] Q.L. Zou, Y.C. Lu, Solvent-dictated lithium sulfur redox reactions: an operando UV-vis spectroscopic study, *J. Phys. Chem. Lett.* 7 (2016) 1518–1525.
- [69] K.H. Wujcik, D.R. Wang, A. Raghunathan, M. Drake, T.A. Pascal, D. Prendergast, N. P. Balsara, Lithium polysulfide radical anions in ether-based solvents, *J. Phys. Chem. C* 120 (2016) 18403–18410.
- [70] C. Barchasz, F. Molton, C. Duboc, J.C. Lepretre, S. Patoux, F. Alloin, Lithium/sulfur cell discharge mechanism: an original approach for intermediate species identification, *Anal. Chem.* 84 (2012), 3973–3980.
- [71] X.F. Yang, X.J. Gao, Q. Sun, S.P. Jand, Y. Yu, Y. Zhao, X. Li, K. Adair, L.Y. Kuo, J. Rohrer, J.N. Liang, X.T. Lin, M.N. Banis, Y.F. Hu, H.Z. Zhang, X.F. Li, R.Y. Li, H. M. Zhang, P. Kaghazchi, T.K. Sham, X.L. Sun, Promoting the transformation of

Li_2S_2 to Li_2S : significantly increasing utilization of active materials for high-sulfur-loading Li-S Batteries, *Adv. Mater.* 31 (2019), 1901220.

- [72] J. Conder, R. Bouchet, S. Trabesinger, C. Marino, L. Gubler, C. Villevieille, Direct observation of lithium polysulfides in lithium-sulfur batteries using operando X-ray diffraction, *Nat. Energy* 2 (2017) 17069.
- [73] S.S. Zhang, Liquid electrolyte lithium/sulfur battery: fundamental chemistry, problems, and solutions, *J. Power Sources* 231 (2013) 153–162.
- [74] M. Wild, L. O'Neill, T. Zhang, R. Purkayastha, G. Minton, M. Marinescu, G.J. Offer, Lithium sulfur batteries, a mechanistic review, *Energy Environ. Sci.* 8 (2015) 3477–3494.
- [75] F.Y. Fan, W.C. Carter, Y.M. Chiang, Mechanism and kinetics of Li_2S precipitation in lithium-sulfur batteries, *Adv. Mater.* 27 (2015) 5203–5209.



Guoran Li is Professor in Institute of New Energy Material Chemistry, Nankai University. His main research interest is focused on new energy materials for hybrid solar cells and rechargeable batteries. He received a Bachelor degree in Chemistry and a PhD degree in Physical Chemistry from Nankai University, respectively, in 2000 and 2005. He worked in Queensland University of Technology as an Endeavour Research Fellow in 2008, and as a visiting professor in Department of Materials Science and Metallurgy, University of Cambridge from 2014 to 2015.



Lu Wang is currently pursuing her doctorate in Prof. Xue-Ping Gao's group in School of Materials Science and Engineering, Nankai University, China. She got her master's degree and bachelor's degree in Nankai University and Qingdao University, respectively. Her research interests mainly include Li-S battery and perovskite solar cell.



Sheng Liu is an Associate Professor in Institute of New Energy Material Chemistry, School of Materials Science and Engineering, Nankai University, China. He received his doctorate at College of Chemistry from Nankai University in 2012. His main research interests include Li-S and Li-ion batteries.



Zhen-Yu Wang received his bachelor's degree of chemistry (2016) at Ocean University of China. He is currently carrying out his Ph.D. research with Prof. Xue-Ping Gao at Nankai University. His research interests focus on the design and build of the cathode in Li-S battery.



Xue-Ping Gao is Professor in Institute of New Energy Material Chemistry, Nankai University of China. He received his doctorate at Department of Chemistry from Nankai University in 1995. He used to work as a visiting research fellow at Kogakuin University in Japan from 1997 to 1999. Currently, his main research is focused on energy storage materials for power sources, including Li-S battery, Li-ion batteries, and solar rechargeable battery.



Jun-Feng Wu got his bachelor's degree from College of Science, Henan Agricultural University. He is now a master student in Prof. Tian-Ying Yan's group in School of Materials Science and Engineering, Nankai University. His research mainly focuses on the high-performance lithium-sulfur battery with advanced functional materials.